Fano Interference between Localized Plasmons and Interface Reflections

ARTICLE *in* ACS NANO · JULY 2012

Impact Factor: 12.88 · DOI: 10.1021/nn302879j · Source: PubMed

2 AUTHORS, INCLUDING:

Mikael Svedendahl
ICFO Institute of Photonic Sciences
23 PUBLICATIONS **372** CITATIONS

Fano Interference between Localized Plasmons and Interface Reflections

Mikael Svedendahl and Mikael Käll*

Department of Applied Physics, Chalmers University of Technology, 412 96 Göteborg, Sweden

ABSTRACT Layers of subwavelength metal nanostructures that support localized surface plasmon resonances are of broad interest in applied nanotechnology, for example, in optical sensor development and solar energy harvesting devices. We measured specular reflection spectra as a function of incidence angle for two-dimensional layers of gold nanodisks on glass and found highly asymmetric line-shapes and a spectral red-shift of up to 0.2 eV, or 10% of the plasmon resonance energy, as the angle changed from normal toward grazing incidence. This dramatic angular dispersion is the result of a tunable Fano interference between the spectrally narrow plasmon emission and a "white" continuum caused by the interface reflection. The data are found to be in excellent agreement with predictions based on a theory for Fresnel reflection coefficients of an interface with subwavelength inclusions. The theory can also be used to derive analytical expressions for the Fano parameters.

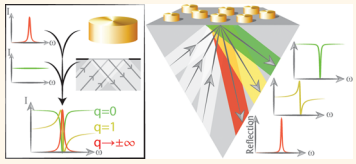

KEYWORDS: Fano resonance · localized surface plasmon · metamaterial · angular dispersion · optical properties

The strong interaction between light and metal nanoparticles that support localized surface plasmon resonances (LSPRs) can be utilized for numerous applications, including a range of molecular sensing and spectroscopy schemes, solar energy harvesting, and development of metamaterials with fascinating optical properties.[1−6] The LSPR originates from the collective motion of the free electrons that are confined within the metal nanoparticle. In the most basic description of the phenomenon, the incident oscillating electric field drives the electron gas as an incompressible fluid back and forth within the particle against the restoring force of the positive ions and the friction caused by electron scattering events. The electron gas then essentially responds as a damped harmonic oscillator and the response function, that is, the particle polarizability, thus has a Lorentzian form. However, over the past few years, it has become apparent that many plasmonic resonances have highly asymmetric line-shapes that are better described by a Fano function:

$$I_F(\omega) = A_F\frac{(q\gamma+\omega-\omega_0)^2}{(\omega-\omega_0)^2+\gamma^2}+B \qquad (1)$$

Here A_F is the resonance amplitude, B is a background term, ω_0 is the resonance frequency, γ is the resonance half-width, and q is the so-called Fano asymmetry parameter. The Fano function is named after Ugo Fano, of atomic physics fame,[7] and appears whenever there is a coherent mixing, or interference, between a discrete (Lorentzian) resonance and a spectrally broad continuum. Since the phase of the discrete oscillator varies rapidly with frequency around ω_0, while the continuum exhibits a constant phase, there will typically be spectral regions of constructive and destructive interference between the two components on opposite sides of the resonance frequency. This is the basic reason behind the asymmetric line-shape. The relative strength of the two contributions is parametrized through q in such a way that the discrete resonance dominate for $|q| \gg 1$, resulting in a Lorenzian peak on top of a weak background, while $|q| = 0$ corresponds to a spectral dip, or an "anti-resonance", in the continuum.[8] The degree of asymmetry is maximal for $q = \pm 1$.

Fano line-shapes have been observed for a range of plasmonic systems that involve some form of interaction between broad and narrow spectral features; see ref 9 for a recent comprehensive review. Many examples involve interactions between narrow multipolar or otherwise "dark" LSPRs and radiatively broadened dipolar plasmons in single particles,[10,11] particle clusters,[12,13] or metamaterials[14−16] or the interaction between narrow diffractive resonances and broad plasmon modes in various arrays or grating structures,[17,18] but Fano interference can also appear due to the interaction between an interband continuum and a dipolar LSPR.[19] Here we report on an optical reflectivity study of gold nanodisks fabricated using hole-mask colloidal lithography (HCL) on glass substrates. These nanodisks

* Address correspondence to mikael.kall@chalmers.se.

Received for review June 28, 2012 and accepted July 18, 2012.

Published online July 18, 2012
10.1021/nn302879j

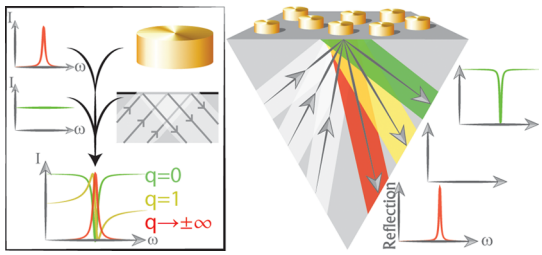

Figure 1. Schematic illustration of Fano interference between localized plasmons and an interface reflection. In a first approximation, the reflection from the supported nanoparticle layer can be thought of as the spectral interference of the Lorenzian scattering from the nanoparticles and the flat "continuum" from the interface reflection. Depending on the individual weights and phases of the two components, which are parametrized through the Fano parameter *q*, the interference can result in a peak, a dip, or a highly asymmetric line-shape.

support a single dipolar plasmon resonance at ~1.9 eV (~650 nm), well below the interband region in gold, but no higher order modes. The particles are separated from each other by approximately a particle diameter, which means that near-field coupling is very weak, and there is no long-range periodicity, which means that there are no diffractive resonances present. Still, we found that the measured reflectivity spectra exhibit a highly pronounced Fano interference that sensitively depends on the excitation geometry and that leads to large spectral shifts and distinct line-shape asymmetries. In the following, we characterize and explain this phenomenon in terms of an interference between the spectrally narrow dipolar LSPR of the gold nanodisks and a "white" continuum caused by the reflection from the intervening glass/air interface. As schematically outlined in Figure 1, the interference can lead to a spectral peak, a dip, or a strongly asymmetric line-shape depending on the relative strength and phase of the two constituents. We believe that the observed effect is not only a particularly simple and attractive example of Fano interference in plasmonics but also an effect of potentially high practical importance. HCL samples have found widespread use in applied nanoplasmonics, in particular in the sensing field,[20−27] but there are, of course, a range of other fabrication methods that also result in plasmonic particles on transparent supports.[28−30] Understanding the spectral properties of such layers is therefore of high importance to plasmonics and applied nanotechnology in general.

RESULTS AND DISCUSSION

Samples and Experiments. We fabricated Au nanodisks with diameter D = 120 nm and height h = 20 nm on standard SiO_2 cover glass through hole-mask colloidal lithography;[31] see Figure 2A. Because of the self-assembly fabrication process, in which the charged colloidal beads arrange laterally due to electrostatic repulsion, HCL samples exhibit only short-range spatial

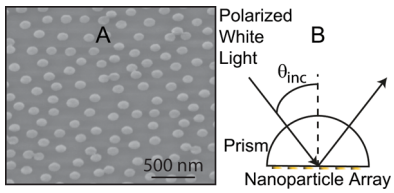

Figure 2. (A) Scanning electron micrograph of gold nanodisks on glass; (B) schematic of the experimental measurement configuration.

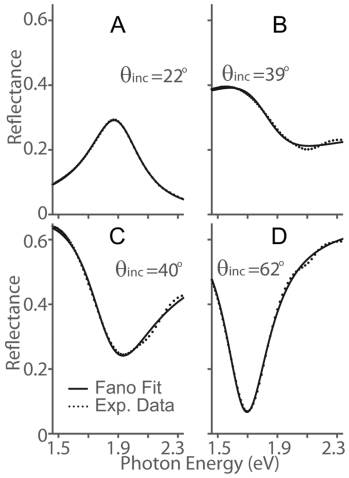

Figure 3. Specular reflection spectra for angles of incidence θ_i = 22°, 39°, 40°, and 62°. Note the asymmetric line-shapes for angles close to the critical angle of the glass−air interface, θ_c = 41.1°. Dotted lines correspond to experimental data, and solid lines are fits to the Fano formula, eq 1.

order. Thus, there is a well-defined nearest neighbor distance but no long-range periodicity. The rather large edge-to-edge separation between neighboring particles, on the order of a particle diameter or more, and the lack of long-range coherent interactions between particles means that both near-field and diffractive coupling effects are weak.[32]

Figure 2B illustrates the experimental setup used. The sample was mounted on a hemispherical prism using indexed matched oil and was illuminated using collimated and polarized white light from a halogen source. The collected spectra were analyzed using a computer-controlled fiber-coupled spectrometer. All data presented here refer to a sample with an average of 12.6 nanodisks per μm^2 and concerns the case of specular reflection. As we have previously shown for samples of similar density,[20] the diffuse scattering from the nanoparticles is then very weak, and the specular reflection spectra therefore represent essentially all light emitted toward the glass side of the interface.

Experimental Reflection Spectra. Figure 3 illustrates our main experimental observations. The figure shows typical specular reflection spectra measured for different angles of incidence using s-polarized light. For the lowest angle, θ_i = 22°, one sees a characteristic and rather symmetric LSPR peak centered at about 1.9 eV

due to the coherent scattering from the nanodisks in the specular direction. In contrast, the reflection spectrum for the highest incidence angle, Figure 3D, θ_i = 62°, instead exhibits a dip because the LSPRs now absorb light that would have been totally internally reflected if the gold nanodisks were not present. The dip is still symmetric, but it is narrower and redshifted by ~0.2 eV compared to the peak in Figure 3A. The most dramatic spectral changes, however, occur for incidence angles close to the critical angle of the air−glass interface, θ_c = 41.1°. As can be seen in Figure 3B and C, the LSPR spectrum is then extremely asymmetric and highly sensitive to the precise angle of incidence. However, all spectra, from the lowest to the highest angles of incidence, can be described by the Fano line-shape function, as shown by the excellent fits of eq 1 to the experimental data in Figure 3. In the following, we present a theoretical model that explains the experimental observations, including the spectral angular dispersion and asymmetry, and that can be used to derive analytical expressions for the Fano line-shape parameters.

Theoretical Reflection Spectra. We model the experimental system described above by combining two theories: the quasistatic dipole polarizability theory for ellipsoids,[33] which is used to describe the optical response of an isolated nanodisk, and the so-called island film theory,[34] which can be used to describe the reflection and transmission properties of a two-dimensional layer of subwavelength inclusions sandwiched between two homogeneous media.

To describe the optical properties of an isolated nanodisk, it is convenient to start from the polarizability model for an oblate spheroid corrected for scattering losses due to finite-size effects.[32,33,35] The dipole polarizability is then exclusively determined by the shape and size of the nanodisk and by the dielectric response of the metal and the surrounding medium. By assuming that the metal can be described by a Drude dielectric function within the photon energy range of interest, it can be shown that the polarizability takes an essentially Lorentzian form:[36]

$$\alpha(\omega) \approx \frac{A}{\omega_{LSPR}^2 - \omega^2 - i\omega(\gamma_0 + F\omega^2)} \qquad (2)$$

Here $A = V\omega_{LSPR}^2/L$ is an amplitude determined by the localized surface plasmon resonance frequency ω_{LSPR} and the volume of the nanodisk V. L is a geometrical depolarization factor fixed by the nanoparticle aspect ratio and includes substrate interactions accounted for through the image dipole theory.[34,37] The resonance frequency is in turn $\omega_{LSPR}^2 = \omega_p^2 L/(\varepsilon_{eff}(1 - L) + L)$, where $\omega_p \approx 1.3 \times 10^{16}$ rad/s is the bulk plasma frequency of gold[38] and ε_{eff} is an effective dielectric constant characterizing the surrounding medium. For an oblate spheroid with the same dimensions as our nanodisks, that is, with radius a = 60 nm and height h = 20 nm, one obtains $L \approx 0.09$ for the long-axis polarizability component. The width of the resonance is determined by the resistive Drude damping factor $\gamma_0 \approx 2.5 \times 10^{13}$ rad/s[38] and a factor $F = \omega_{LSPR}^2 a^2 h/9c^3 L$ that describes the radiative damping contribution that arises due to the finite size of the particle. In the following, we will make the simplifying assumption that the optical response of a single nanodisk is completely dominated by the long-axis polarizability components, that is, by the polarization within the plane of the interface. This means that we need to consider only one plasmon resonance, an assumption that is justified by the fact that the short-axis resonances of gold nanodisks have weak intensities and occur at higher frequencies than considered here.

The island film theory has previously been shown to give an excellent representation of ellipsometry data for HCL samples.[37] The theory is based on modifications of the boundary conditions for the electromagnetic fields at an interface between two homogeneous media. The modifications take into account excess current and charge densities present due to discrete subwavelength "islands" at the boundary and result in modified Fresnel coefficients for the interface. In the Supporting Information, we briefly outline the derivation of these coefficients following Bedeaux and Vlieger.[34] We consider a plane wave propagating through a medium with refractive index n_i (here $n_i = n_{glass}$ = 1.52) toward a boundary against a medium with refractive index n_t (here $n_t = n_{air}$ = 1). With the incident electric field $\vec{E}_i$ pointing along the interface, that is, the case of s-polarization, the result for the reflection coefficient is

$$r_s = E_i/E_r = \frac{n_i \cos\theta_i - n_t \cos\theta_t + i\frac{\omega}{c}\rho\alpha(\omega)}{n_i \cos\theta_i + n_t \cos\theta_t - i\frac{\omega}{c}\rho\alpha(\omega)} \qquad (3)$$

Here θ_i and θ_t are the angles of incidence and transmission, respectively, and $\rho\alpha(\omega)$ defines the total optical density of the interface through the frequency-dependent polarizability, $\alpha(\omega)$, of a single nanoparticle "island" and the surface density of nanoparticles, ρ. Similarly, the reflection coefficient for p-polarized light can be derived. With the assumption that the polarizability perpendicular to the interface can be neglected, the result is

$$r_p = \frac{n_t \cos\theta_i - n_i \cos\theta_t - i\frac{\omega}{c}\rho\alpha(\omega)\cos\theta_i \cos\theta_t}{n_t \cos\theta_i + n_i \cos\theta_t - i\frac{\omega}{c}\rho\alpha(\omega)\cos\theta_i \cos\theta_t} \qquad (4)$$

Comparing Theory and Experiments. A simulation of the angular and polarization-dependent reflectance spectra from our samples based on eq 3 and eq 4 requires only that the frequency-dependent average optical

density $\rho\alpha(\omega)$ of the interface is known. In the following, we determine $\rho\alpha(\omega)$ from a simple transmission measurement taken at normal incidence and then use this result to predict the angular variation of the reflection spectra and line-shape parameters for arbitrary angles of incidence.

Figure 4 shows the experimental transmission spectrum for the sample shown in Figure 2 together with a curve-fit to

$$T(\theta_i = 0) = \frac{4n_i n_t}{\left| n_i + n_t - i\frac{\omega}{c}\rho\alpha(\omega) \right|} \quad (5)$$

which can be derived along the same lines as eqs 3 and 4. The functional form used for $\rho\alpha(\omega)$ is the Lorentzian

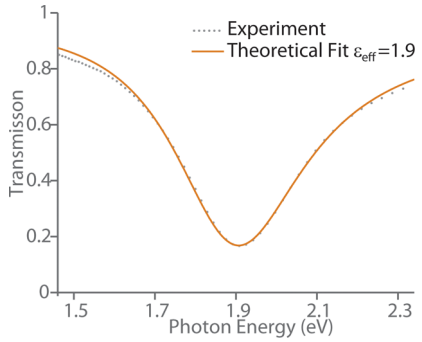

Figure 4. Experimental transmission spectrum for the sample shown in Figure 2A taken at normal incidence. The full curve shows a theoretical spectrum according to eq 5 based on modeling $\alpha(\omega)$ using eq 2 by adjusting a single free parameter, that is, the effective dielectric constant surrounding the nanoparticles, ε_{eff}.

in eq 2, where we used the actual nanodisk dimensions and surface density for our sample and the Drude parameters mentioned above to characterize the metal dielectric function. Thus, the only adjustable parameter is the average dielectric constant ε_{eff} affecting the nanodisks, which is needed to obtain the resonance at the correct spectral location. We find excellent agreement between theory and experiment for ε_{eff} = 1.9, which is a reasonable result for gold nanodisks on glass in air.

Figure 5 summarizes the experimental reflection spectra for s- and p-polarization as a function of incidence angle for the sample shown in Figure 2A together with corresponding theoretical spectra based on utilizing the $\alpha(\omega)$ retrieved from the transmission measurement shown in Figure 4. The figure shows the data as surface plots with the reflectivity of each spectrum normalized to the same color bar in order to highlight the angular dependence of the most distinct spectral features. The excellent agreement between the experiment and theory should be quite clear. For example, the model clearly captures the pronounced spectral dispersion for large incidence angles seen for s-polarized light, the dramatic spectral asymmetry associated with the transition from a spectral "peak" to a "dip" around θ_c, and even the slight blue-shift of the dip just above the critical angle seen for p-polarized incidence. We take this agreement as evidence that the theoretical analysis described above contains the essential physics of the observed phenomenon.

To explain the results summarized in Figure 5, one needs to take into account the interference between

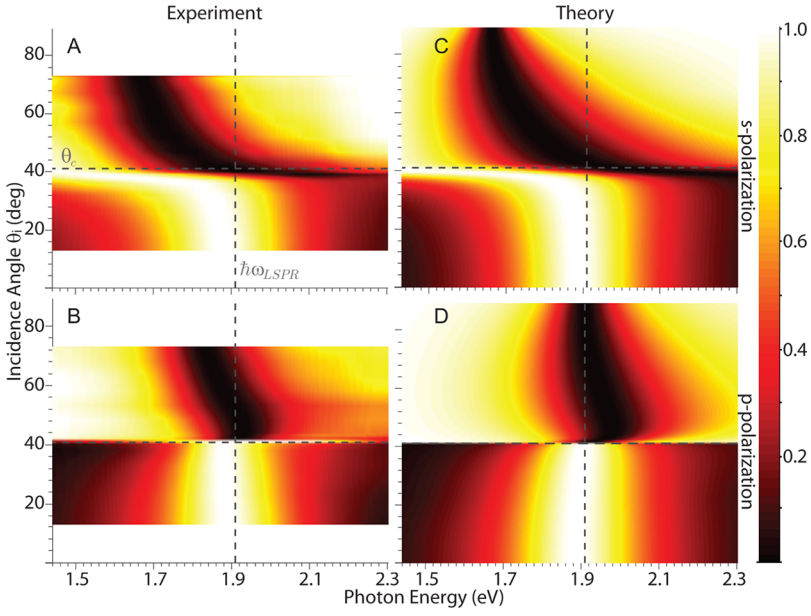

Figure 5. Normalized experimental and theoretical reflection spectra. The s-polarized reflection line-shapes (A, C) from the Au nanodisk array in Figure 2A show a greater dispersion with incidence angle than the p-polarized spectra (B, D). Note the strongly asymmetric line-shapes for angles slightly smaller than the critical angle for the s-polarized case. The limited angular range of the measured spectra is due to constraints in the experimental setup. Dashed lines show the Lorentzian resonance energy, $\hbar\omega_{LSPR}$, (vertical), and the critical angle for the bare interface, θ_c (horizontal).

the two components that build up the reflection spectra, that is, the white "continuum" originating from the bare interface reflection and the coherent scattering from the nanoparticle layer in the specular direction, as indicated in Figure 1.[39] Both components vary in relative amplitude and phase as a function of incidence angle, photon energy, and polarization, and this variation, quantified through eqs 3 and 4, is the ultimate cause behind the spectral variation. For example, the strong spectral dispersion for s-polarization above θ_c is a consequence of the gradually increasing phase shift of the continuum component (which varies from 0 for $\theta_i = \theta_c$ to π at $\theta_i = 90°$ relative to the incident field) and the spectrally varying phase shift of the particle component (from 0 for $\hbar\omega \ll \hbar\omega_{LSPR}$ to π for $\hbar\omega \gg \hbar\omega_{LSPR}$), which result in maximum destructive interference (the position of the "dip") at photon energies that decrease rapidly with increasing incidence angle. This effect is not as pronounced for p-polarization because of the less efficient excitation of the LSPR, which is driven only by the in-plane component of the transmitted field. This component is zero at θ_c and always smaller than in the s-polarized case. One can understand the pronounced spectral dispersion for angles $\theta_i < \theta_c$ seen for s-polarized spectra along similar lines. However, in this case the dominant cause is the angular variation of the continuum amplitude, which would vary from $r = (n_i - n_t)/(n_i - n_t) \approx 0.2$ at normal incidence to 1 at $\theta_i = \theta_c$ in the case of a bare glass–air interface, while the amplitude of the particle contribution does not vary significantly with angle for an s-polarized driving field, and the phase of the continuum is constant (r is real for $\theta_i < \theta_c$). The angle-dependent relative amplitude of the two contributions and the spectral variation of the phase of the particle contribution thus determine the degree of interference. For a particle density that is sufficiently high, the result is a transition from a spectral peak to a dip at a transition angle slightly smaller than the critical angle, while a particle layer with low optical density would not show a peak at any angles of incidence. Exactly at the transition angle, the two contributions interfere constructively just below and destructively just above the LSPR resonance frequency, leading to a maximum degree of spectral asymmetry. This effect is illustrated by the spectrum in Figure 3B.

The qualitative interpretation of the spectral trends given above can also be quantified in terms of the Fano resonance parameters mentioned in the introduction. For the particular case of a strictly Lorentzian particle polarizability, one can *exactly* map R_p and R_s on the Fano formula, eq 1. Using this approach, we have derived analytical expressions for the Fano parameters q, γ, E_0, E_{min}, and E_{max}, as described in the Supporting Information. However, the line-shape function used as a basis for the theoretical spectra in Figure 5, that is,

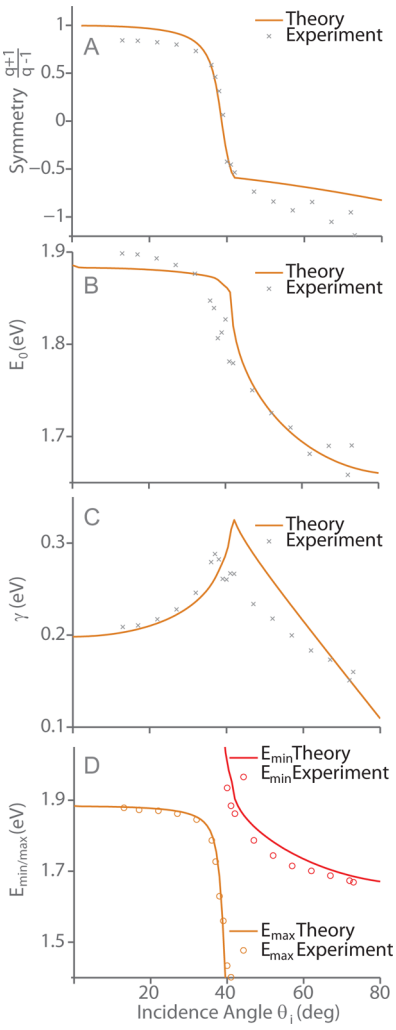

Figure 6. Comparison between the Fano parameters acquired analytically, using eq 2 as a model for $\alpha(\omega)$, and experimentally acquired parameters. The angular variations of the symmetry (A), resonance energy (B), and spectral width (C) are parameters of the Fano line-shape, yielding spectra with distinct spectral minima and maxima (D).

eq 2, deviates slightly from a perfect Lorentzian because of the frequency-dependent radiative decay term $F\omega^2$, which introduces a weak "intrinsic" line-shape asymmetry that makes an analytical mapping extremely cumbersome. In Figure 6, we instead show the angular dependence of q, γ, E_0, E_{min}, and E_{max} obtained from fitting the experimental and theoretical s-polarized angular-dependent reflection measurements shown in Figures 3 and 5 to eq 1. We have here chosen to plot the degree of asymmetry as $(q - 1)/(q + 1)$, where q is the Fano parameter, in order to avoid divergences. The figure again illustrates the good agreement between the experimental results and the theoretical spectra, which nicely captures the crucial line-shape variations with angle, although the only real fitting parameter we have used is the effective refractive index surrounding the nanoparticles. The deviations that do appear can of course have many origins,

including inhomogeneous broadening, weak interparticle coupling effects, a small contribution from the vertical polarizability of the particle layer, and finite spectral and angular resolution of the experimental setup, but none of these effects obviously have any major influence on the overall spectral properties.

CONCLUDING REMARKS

To summarize, we have shown that the specular reflections from short-range ordered nanoplasmonic particle arrays on a dielectric interface can result in highly dispersive and asymmetric resonance lineshapes that are extremely sensitive to the angle of incidence. The effect can be understood as a Fano interference between the essentially Lorentzian nanoparticle scattering spectrum and the flat continuum comprising the dielectric interface reflectance. We found excellent quantitative agreement between experimental data and a theory based on modified Fresnel reflection coefficients.

The results described herein should be useful from a practical point of view because they offer a simple quantitative framework for how to analyze, predict, and optimize the spectroscopic characteristics of plasmonic particle layers in general. One application example could be nanoplasmonic biosensing experiments, which often suffer from unspecific binding of biomolecules on the glass separating the plasmonic particles. We can, for example, predict that this effect will lead to a small change in the reflectivity of the glass surface that will couple to the measured plasmon spectrum through the Fano interference, thereby potentially leading to ambiguities in interpretation of spectral shifts. Another application in sensing could be to utilize the large phase differences between p- and s-polarized spectra induced by the Fano interference to generate mixed polarization states that are more sensitive to a change in the plasmonic resonance than ordinary transmission or reflectance spectra.[25] The results also lead to questions of more fundamental character. For example, one may ask how the strong spectral dispersion with angle, which would typically be taken as evidence for plasmon delocalization and propagation, can be reconciled with the fact that the observed effects can be explained without invoking any explicit interparticle interactions. It would of course also be interesting to be able to relate the observed far-field effects to a detailed picture of optical near-fields and currents at the level of a single particle. Finally, we note that a recent theory of perfect optical absorption by Garcia de Abajo and co-workers[39] is essentially analogous to the interference model we have used here. In particular, perfect absorption will appear as a complete Fano anti-resonance for certain particle densities and angles in both s- and p-polarized spectra. We hope to come back to this and several of the other issues mentioned above in future publications.

METHODS

Fabrication of Au Nanodisks. The HCL fabrication technique is based on first depositing colloidal polystyrene beads through self-assembly on a substrate covered by PMMA. A thin gold film is then deposited on the sample, the polystyrene beads are removed by tape stripping, and the thus exposed PMMA is etched away down to the substrate. Subsequent metal deposition and removal of the hole-mask result in the substrate being covered with cylindrical metal particles with diameters predetermined by the diameter of the polystyrene beads used and the height defined by the amount of deposited metal.

Optical Measurements. The sample was mounted on a hemispherical prism (BK7, refractive index $n_p \approx 1.52$) using indexed matched oil (refractive index $n_o \approx 1.52$) and centered above a rotational stage that allowed for exact tuning of the angle of incidence θ_i. The array was illuminated using a beam of collimated (divergence below 0.4°) and polarized white light from a halogen source. A second rotational stage containing the collection optics was used to define the collection angle $\theta_{coll.}$. All results refer to the case of specular reflection; that is, $\theta_{coll.} = \theta_i$. The reflected light was collected by a fiber-coupled spectrometer (B&WTek BRC711E), and the recorded spectra were normalized to the totally reflected light from a bare glass sample placed in the sample position.

Conflict of Interest: The authors declare no competing financial interest.

Acknowledgment. We are grateful to S. Chen and G. Zengin for providing samples and to P. Johansson and J. Garcia de Abajo for stimulating comments and discussions. This work was financially supported by Vinnova, the Swedish Foundation for Strategic Research, and the Swedish Research Council.

Supporting Information Available: Derivations of reflection coefficients and Fano parameters are described. This material is available free of charge *via* the Internet at http://pubs.acs.org.

REFERENCES AND NOTES

1. Anker, J. N.; Hall, W. P.; Lyandres, O.; Shah, N. C.; Zhao, J.; Van Duyne, R. P. Biosensing with Plasmonic Nanosensors. *Nat. Mater.* **2008**, *7*, 442–453.
2. Kamat, P. V. Photophysical, Photochemical and Photocatalytic Aspects of Metal Nanoparticles. *J. Phys. Chem. B* **2002**, *106*, 7729–7744.
3. Atwater, H. A.; Polman, A. Plasmonics for Improved Photovoltaic Devices. *Nat. Mater.* **2010**, *9*, 205–213.
4. Maier, S. A.; Brongersma, M. L.; Kik, P. G.; Atwater, H. A. Observation of Near-Field Coupling in Metal Nanoparticle Chains Using Far-Field Polarization Spectroscopy. *Phys. Rev. B* **2002**, *65*, 4.
5. Yao, J. M.; Le, A. P.; Gray, S. K.; Moore, J. S.; Rogers, J. A.; Nuzzo, R. G. Functional Nanostructured Plasmonic Materials. *Adv. Mater.* **2010**, *22*, 1102–1110.
6. Lal, S.; Link, S.; Halas, N. J. Nano-Optics from Sensing to Waveguiding. *Nat. Photonics* **2007**, *1*, 641–648.
7. Fano, U. Effects of Configuration Interaction on Intensities and Phase Shifts. *Phys. Rev.* **1961**, *1*, 1866–1878.
8. Miroshnichenko, A. E.; Flach, S.; Kivshar, Y. S. Fano Resonances in Nanoscale Structures. *Rev. Mod. Phys.* **2010**, *82*, 2257–2298.
9. Luk'yanchuk, B.; Zheludev, N. I.; Maier, S. A.; Halas, N. J.; Nordlander, P.; Giessen, H.; Chong, C. T. The Fano Resonance in Plasmonic Nanostructures and Metamaterials. *Nat. Mater.* **2010**, *9*, 707–715.

10. Luk'yanchuk, B. S.; Tribelsky, M. I.; Ternovsky, V.; Wang, Z. B.; Hong, M. H.; Shi, L. P.; Chong, T. C. Peculiarities of Light Scattering by Nanoparticles and Nanowires Near Plasmon Resonance Frequencies in Weakly Dissipating Materials. *J. Opt. A, Pure Appl. Opt.* **2007**, *9*, S294–S300.
11. Mukherjee, S.; Sobhani, H.; Lassiter, J. B.; Bardhan, R.; Nordlander, P.; Halas, N. J. Fanoshells: Nanoparticles with Built-in Fano Resonances. *Nano Lett.* **2010**, *10*, 2694–2701.
12. Lassiter, J. B.; Sobhani, H.; Fan, J. A.; Kundu, J.; Capasso, F.; Nordander, P.; Halas, N. J. Fano Resonances in Plasmonic Nanoclusters: Geometrical and Chemical Tunability. *Nano Lett.* **2010**, *10*, 3184–3189.
13. Fan, J. A.; Bao, K.; Wu, C.; Bao, J.; Bardhan, R.; Halas, N. J.; Manoharan, V. N.; Shvets, G.; Nordlander, P.; Capasso, F. Fano-like Interference in Self-Assembled Plasmonic Ouadrumer Clusters. *Nano Lett.* **2010**, *10*, 4680–4685.
14. Liu, N.; Weiss, T.; Mesch, M.; Langguth, L.; Eigenthaler, U.; Hirscher, M.; Sonnichsen, C.; Giessen, H. Planar Metamaterial Analogue of Electromagnetically Induced Transparency for Plasmonic Sensing. *Nano Lett.* **2010**, *10*, 1103–1107.
15. Verellen, N.; Van Dorpe, P.; Huang, C.; Lodewijks, K.; Vandenbosch, G. A. E.; Lagae, L.; Moshchalkov, V. V. Plasmon Line Shaping Using Nanocrosses for High Sensitivity Localized Surface Plasmon Resonance Sensing. *Nano Lett.* **2011**, *11*, 391–397.
16. Papasimakis, N.; Fu, Y. H.; Fedotov, V. A.; Prosvirnin, S. L.; Tsai, D. P.; Zheludev, N. I. Metamaterial with Polarization and Direction Insensitive Resonant Transmission Response Mimicking Electromagnetically Induced Transparency. *Appl. Phys. Lett.* **2009**, 94.
17. de Abajo, F. J. G. Colloquium: Light Scattering by Particle and Hole Arrays. *Rev. Mod. Phys.* **2007**, *79*, 1267–1290.
18. Kuznetsov, A. I.; Evlyukhin, A. B.; Goncalves, M. R.; Reinhardt, C.; Koroleva, A.; Arnedillo, M. L.; Kiyan, R.; Marti, O.; Chichkov, B. N. Laser Fabrication of Large-Scale Nanoparticle Arrays for Sensing Applications. *ACS Nano* **2011**, *5*, 4843–4849.
19. Pakizeh, T.; Langhammer, C.; Zoric, I.; Apell, P.; Kall, M. Intrinsic Fano Interference of Localized Plasmons in Pd Nanoparticles. *Nano Lett.* **2009**, *9*, 882–886.
20. Svedendahl, M.; Chen, S.; Dmitriev, A.; Kall, M. Refractometric Sensing Using Propagating *versus* Localized Surface Plasmons: A Direct Comparison. *Nano Lett.* **2009**, *9*, 4428–4433.
21. Chen, S.; Svedendahl, M.; Van Duyne, R. P.; Kall, M. Plasmon-Enhanced Colorimetric ELISA with Single Molecule Sensitivity. *Nano Lett.* **2011**, *11*, 1826–1830.
22. Larsson, E. M.; Langhammer, C.; Zoric, I.; Kasemo, B. Nanoplasmonic Probes of Catalytic Reactions. *Science* **2009**, *326*, 1091–1094.
23. Otte, M. A.; Estevez, M. C.; Carrascosa, L. G.; Gonzalez-Guerrero, A. B.; Lechuga, L. M.; Sepulveda, B. Improved Biosensing Capability with Novel Suspended Nanodisks. *J. Phys. Chem. C* **2011**, *115*, 5344–5351.
24. Feuz, L.; Jonsson, M. P.; Hook, F. Material-Selective Surface Chemistry for Nanoplasmonic Sensors: Optimizing Sensitivity and Controlling Binding to Local Hot Spots. *Nano Lett.* **2012**, *12*, 873–879.
25. Lodewijks, K.; Van Roy, W.; Borghs, G.; Lagae, L.; Van Dorpe, P. Boosting the Figure-of-Merit of LSPR-Based Refractive Index Sensing by Phase-Sensitive Measurements. *Nano Lett.* **2012**, *12*, 1655–1659.
26. Vogel, N.; Fischer, J.; Mohammadi, R.; Retsch, M.; Butt, H.-J.; Landfester, K.; Weiss, C. K.; Kreiter, M. Plasmon Hybridization in Stacked Double Crescents Arrays Fabricated by Colloidal Lithography. *Nano Lett.* **2011**, *11*, 446–454.
27. Cataldo, S.; Zhao, J.; Neubrech, F.; Frank, B.; Zhang, C.; Braun, P. V.; Giessen, H. Hole-Mask Colloidal Nano lithography for Large-Area Low-Cost Metamaterials and Antenna-Assisted Surface-Enhanced Infrared Absorption Substrates. *ACS Nano* **2012**, *6*, 979–985.
28. Shalaev, V. M.; Cai, W. S.; Chettiar, U. K.; Yuan, H. K.; Sarychev, A. K.; Drachev, V. P.; Kildishev, A. V. Negative Index of Refraction in Optical Metamaterials. *Opt. Lett.* **2005**, *30*, 3356–3358.
29. Kekatpure, R. D.; Barnard, E. S.; Cai, W. S.; Brongersma, M. L. Phase-Coupled Plasmon-Induced Transparency. *Phys. Rev. Lett.* **2010**, *104*, 4.
30. Fan, J. A.; Wu, C. H.; Bao, K.; Bao, J. M.; Bardhan, R.; Halas, N. J.; Manoharan, V. N.; Nordlander, P.; Shvets, G.; Capasso, F. Self-Assembled Plasmonic Nanoparticle Clusters. *Science* **2010**, *328*, 1135–1138.
31. Fredriksson, H.; Alaverdyan, Y.; Dmitriev, A.; Langhammer, C.; Sutherland, D. S.; Zaech, M.; Kasemo, B. Hole-Mask Colloidal Lithography. *Adv. Mater.* **2007**, *19*, 4297–4302.
32. Hanarp, P.; Kall, M.; Sutherland, D. S. Optical Properties of Short Range Ordered Arrays of Nanometer Gold Disks Prepared by Colloidal Lithography. *J. Phys. Chem. B* **2003**, *107*, 5768–5772.
33. Bohren, C. F.; Huffman, D. R. *Absorption and Scattering of Light by Small Particles*; John Wiley and Sons: New York, 1983.
34. Bedeaux, D.; Vlieger, J. *Optical Properties of Surfaces*; Imperial Collage Press: London, 2001.
35. Wokaun, A.; Gordon, J. P.; Liao, P. F. Radiation Damping in Surface-Enhanced Raman Scattering. *Phys. Rev. Lett.* **1982**, *48*, 957–960.
36. Zoric, I.; Zach, M.; Kasemo, B.; Langhammer, C. Gold, Platinum, and Aluminum Nanodisk Plasmons: Material Independence, Subradiance, and Damping Mechanisms. *ACS Nano* **2011**, *5*, 2535–2546.
37. Mendoza-Galvan, A.; Jarrendahl, K.; Dmitriev, A.; Pakizeh, T.; Kall, M.; Arwin, H. Optical Response of Supported Gold Nanodisks. *Opt. Express* **2011**, *19*, 12093–12107.
38. Blaber, M. G.; Arnold, M. D.; Ford, M. J. Search for the Ideal Plasmonic Nanoshell: The Effects of Surface Scattering and Alternatives to Gold and Silver. *J. Phys. Chem. C* **2009**, *113*, 3041–3045.
39. Thongrattanasiri, S.; Koppens, F. H. L.; Javier Garcia de Abajo, F. Complete Optical Absorption in Periodically Patterned Graphene. *Phys. Rev. Lett.* **2012**, *108*, 047401.